



HAL
open science

In vivo hepatic lipid quantification using MRS at 7 Tesla in a mouse model of glycogen storage disease type 1a

N. Ramamonjisoa, H. Ratiney, E. Mutel, Hervé Guillou, G. Mithieux, F. Pilleul, F. Rajas, O. Beuf, S. Cavassila

► **To cite this version:**

N. Ramamonjisoa, H. Ratiney, E. Mutel, Hervé Guillou, G. Mithieux, et al.. In vivo hepatic lipid quantification using MRS at 7 Tesla in a mouse model of glycogen storage disease type 1a. *Journal of Lipid Research*, 2013, 54 (7), pp.2010-2022. 10.1194/jlr.D033399 . hal-00847703

HAL Id: hal-00847703

<https://hal.science/hal-00847703>

Submitted on 29 May 2020

HAL is a multi-disciplinary open access archive for the deposit and dissemination of scientific research documents, whether they are published or not. The documents may come from teaching and research institutions in France or abroad, or from public or private research centers.

L'archive ouverte pluridisciplinaire **HAL**, est destinée au dépôt et à la diffusion de documents scientifiques de niveau recherche, publiés ou non, émanant des établissements d'enseignement et de recherche français ou étrangers, des laboratoires publics ou privés.

Copyright

In vivo hepatic lipid quantification using MRS at 7 Tesla in a mouse model of glycogen storage disease type 1a

Nirilanto Ramamonjisoa,* Helene Ratiney,^{1,*} Elodie Mutel,[†] Herve Guillou,[§] Gilles Mithieux,[†] Frank Pilleul,^{***,††} Fabienne Rajas,[†] Olivier Beuf,* and Sophie Cavassila*

Université de Lyon,* CREATIS, CNRS UMR 5220, Inserm U1044, INSA-Lyon, Université Lyon 1, Villeurbanne, France; Université de Lyon,[†] Université Lyon 1, Institut National de la Santé et de la Recherche Médicale, U855, Lyon, France; UMR1331,[§] INP, UPS, TOXALIM, INRA, Toulouse, France; Hospices Civils de Lyon,^{**} Département d'imagerie digestive, CHU Edouard Herriot, Lyon, France; and Centre Léon Bérard-Centre de Lutte contre le Cancer,^{††} Lyon, France

Abstract The assessment of liver lipid content and composition is needed in preclinical research to investigate steatosis and steatosis-related disorders. The purpose of this study was to quantify in vivo hepatic fatty acid content and composition using a method based on short echo time proton magnetic resonance spectroscopy (MRS) at 7 Tesla. A mouse model of glycogen storage disease type 1a with inducible liver-specific deletion of the glucose-6-phosphatase gene (*L-G6pc*^{-/-}) mice and control mice were fed a standard diet or a high-fat/high-sucrose (HF/HS) diet for 9 months. In control mice, hepatic lipid content was found significantly higher with the HF/HS diet than with the standard diet. As expected, hepatic lipid content was already elevated in *L-G6pc*^{-/-} mice fed a standard diet compared with control mice. *L-G6pc*^{-/-} mice rapidly developed steatosis which was not modified by the HF/HS diet. On the standard diet, estimated amplitudes from olefinic protons were found significantly higher in *L-G6pc*^{-/-} mice compared with that in control mice. *L-G6pc*^{-/-} mice showed no noticeable polyunsaturation from diallylic protons. Total unsaturated fatty acid indexes measured by gas chromatography were in agreement with MRS measurements. These results showed the great potential of high magnetic field MRS to follow the diet impact and lipid alterations in mouse liver.—Ramamonjisoa, N., H. Ratiney, E. Mutel, H. Guillou, G. Mithieux, F. Pilleul, F. Rajas, O. Beuf, and S. Cavassila. In vivo hepatic lipid quantification using MRS at 7 Tesla in a mouse model of glycogen storage disease type 1a. *J. Lipid Res.* 2013. 54: 2010–2022.

Supplementary key words magnetic resonance spectroscopy • hepatic fatty acid quantification and composition • steatosis

This work was supported by research grants from the Agence Nationale de la recherche (ANR-07-MRAR-011-01), the Association Francophone des Glycogénoses, and Projets Exploratoires/Premier Soutien. N.R. is supported by a Centre National de la Recherche Scientifique grant. This work was performed within the framework of the LabEX PRIMES (ANR-11-LABX-0063) of Université de Lyon, within the program "Investissements d'Avenir" (ANR-11-IDEX-007) operated by the French National Research Agency (ANR).

Manuscript received 18 October 2012 and in revised form 2 April 2013.

Published, JLR Papers in Press, April 16, 2013
DOI 10.1194/jlr.D033399

Glycogen storage disease type 1 (GSD 1) is an autosomal recessive metabolic disorder resulting in severe impairment of glucose production and large accumulation of lipids within hepatocytes (steatosis) (1, 2). The phenotype of GSD 1 results from a defect in the glucose-6 phosphatase (G6Pase) complex, leading to severe hypoglycemia due to the loss of endogenous glucose production. Despite a strict diet, patients with GSD 1 develop hepatomegaly and steatosis and may develop, with age, hepatocellular adenoma that can ultimately evolve into hepatocellular carcinoma (3, 4). Recently, a viable mouse model of GSD 1a with a liver-specific deletion of G6Pase catalytic subunit (*L-G6pc*^{-/-}) has been generated and validated (5). GSD 1a mice exhibit hepatic pathological features very similar to those observed in GSD 1a patients.

The accumulation of lipids in the liver relates to the buildup of neutral lipids, such as triglycerides (TGs) and cholesterol esters, stored as lipid droplets in hepatocytes and leading to hepatic steatosis. This fat accumulation may originate from *a*) peripheral fat stored in adipose tissue that flows to the liver as plasma nonesterified fatty acids, *b*) fatty acids newly made within the liver through de novo lipogenesis, and *c*) dietary fatty acids (6, 7).

Steatosis is highly linked to the development of metabolic diseases such as obesity or type 2 diabetes, but it can also result from genetic disorders impacting lipid and glucose metabolism such as in GSD 1a, α 1-antitrypsin deficiency,

Abbreviations: ChREBP, carbohydrate response element binding protein; CRB, Cramér Rao bound; FAME, fatty acid methyl ester; FU, fraction of unsaturation; GC, gas chromatography; G6Pase, glucose-6 phosphatase; GSD 1, glycogen storage disease type 1; HF/HS, high-fat/high-sucrose; *L-G6pc*^{-/-}, liver-specific knockout of glucose-6 phosphatase catalytic subunit; MRS, magnetic resonance spectroscopy; PRESS, point-resolved spectroscopy; rTUFA, relative total unsaturated fatty acid; SC, saturated component; SFA, saturated fatty acid; SNR, signal-to-noise ratio; TE, echo time; TG, triglyceride; TL, total lipid; TR, repetition time; TUBI, total unsaturated bond index; TUFA, total unsaturated fatty acid; TUFU, total unsaturated fatty acid index.

[†]To whom correspondence should be addressed.
e-mail: helene.ratiney@creatis.univ-lyon1.fr

or tyrosinemia type 1. Recent studies suggest a crucial importance of hepatic fatty acid composition in the metabolic consequences of steatosis. Indeed, the harmful effects of several fatty acids, and particularly, of palmitate on insulin signaling are well documented (8, 9). In rats, the enrichment of oleate in the diet is associated with improved insulin sensitivity (10). Interestingly, the overexpression of a constitutively active form of the lipogenic factor, carbohydrate response element binding protein (ChREBP), improves glycemic control and restores hepatic insulin sensitivity in obese and diabetic mice despite an exacerbation of hepatic lipid accumulation. These improvements are associated with an increased oleate/palmitate ratio in the livers of mice overexpressing ChREBP (11). These studies illustrate that it is important to detect lipids accumulating in steatosis but also to profile fatty acids in order to predict damages to the organ.

To date, a liver biopsy is necessary to analyze the fatty acid composition, commonly performed by gas chromatography (GC), a technique requiring the extraction and preparation of tissue samples (12). However, a liver biopsy is an invasive and painful technique that can lead to false negative results (13), and is not suitable for longitudinal studies.

While ^1H -magnetic resonance spectroscopy (MRS) has extensively been used as a noninvasive reference method to assess total fat content, recent studies have demonstrated its ability to assess *in vivo* TG composition (14).

In animal studies, MRS has been used to assess diet impact on lipid composition in the liver (15) and adipose tissue (16, 17) as well as in the muscle of a diabetic mouse model (18). Many other animal models are available to investigate steatosis, such as the genetic model *ob/ob* mouse. The *ob/ob* mouse model develops steatosis spontaneously and has been well studied by ^1H -MRS (19–22). Mice fed a high-fat or a high-fructose diet were also reported with steatosis (23, 24).

At high magnetic fields [≥ 3 Tesla (T)], which allows a better spectral dispersion, ^1H -MRS has also been used to characterize lipid accumulation and lipid composition in a rat model of liver fibrosis (25), or to evaluate fat content in diabetic obese rats (26) and mice (22). Recently, this technique was correlated with histology and TG level (21) in order to compare these techniques for fat quantification in mice. At clinical fields (≤ 3 T), the TG composition of subcutaneous human adipose tissue has been estimated and validated with GC (27).

In this paper, localized short echo time (TE) *in vivo* MRS and GC analysis was used to evaluate the content and composition of fatty liver in *L-G6pc*^{-/-} mice as well as in control *C57BL/6j* mice. *L-G6pc*^{-/-} and control mice were fed either a standard diet or a high-fat/high-sucrose (HF/HS) diet to compare genetically induced steatosis and diet-induced steatosis. *In vitro* validation of the proposed method was first conducted before its application. The method was based on respiratory-gated localized short TE and an automated time-domain quantification method employing a nonlinear least-squares algorithm that fits the time-domain signal to a Voigt model function and uses multiple random starting values and bounds.

In this study, a whole MRS-based procedure was described and validated to quantify noninvasively the hepatic fat content and composition, and determine the possible impact of the diet on the hepatic lipid composition in *L-G6pc*^{-/-} and control mice.

METHOD

Animal groups

The induction of the *G6pc* exon 3 was performed at adult age (7–8 weeks of age) by treating female B6.SA^{CreERT2}.*G6pc*^{lox/lox} mice with tamoxifen (5). After *G6pc* deletion, mice were fed either a standard diet (3.1% lipids, 60% carbohydrates, 16.1% proteins) ($n = 15$) or a HF/HS diet (36.1% lipids, 35% carbohydrates, 19.8% proteins) ($n = 12$) during 9 months. The detailed composition of the diet was previously described by Moraes et al. (28). Two groups of control mice (*C57Bl6/j*; Charles Rivers Laboratories, France) fed a standard ($n = 5$) or a HF/HS ($n = 12$) diet were also analyzed. All animals were housed in the animal facility of Université Lyon 1 (Animaleries Lyon Est Conventiennelle et SPF), under controlled temperature (22°C), with a 12 h light-12 h dark cycle. Mice had free access to food and water. The experiments were conducted according to the procedures approved by the Institutional Animal Care and Ethical Committee of Lyon 1 University. Following MR examinations, a subset of mice was killed by dislocation of the cervical vertebrae and liver tissue samples were rapidly removed and frozen using tongs previously chilled in liquid N₂ to analyze lipids by GC and to quantify TG levels using a Biomérieux colorimetric kit.

MR experimental conditions

Magnetic resonance imaging and magnetic resonance spectroscopic data were collected on a 7 Tesla Biospec 70/20 system (Bruker, Ettlingen, Germany) equipped with a shielded gradient set (400 mT·m⁻¹ maximum gradient amplitude and 120 mm inner diameter) and a ^1H transmit-receive quadrature coil (Rapid Biomedical, Würzburg, Germany) with 32 mm inner diameter. Animals were anesthetized by inhalation of 2% isoflurane. The body temperature was maintained inside the magnet at 37°C by warm water circulation. A pressure sensor was used to monitor the respiratory cycle. A point-resolved spectroscopy (PRESS) sequence was used for localized ^1H -MRS with a short TE (16 ms). The effective repetition time (TR), which had to be a multiple of the respiratory period of the mouse, was set to be greater than 3 s to minimize T1 relaxation effects. The prescription of the voxel ($3 \times 3 \times 3$ mm³) localization within the right lobe of the liver in an area free of large hepatic vessels and surrounding fat, was done on the T2-weighted RARE (Rapid Acquisition with Relaxation Enhancement) images that were previously acquired with the following parameters: TE, 40.4 ms; field of view, 30×30 mm²; matrix, 256×192 ; 36 or 48 slices; slice thickness, 0.5 mm; RARE factor, 8. The sequence was synchronized with respiration using balanced acquisitions over several respiratory periods with an effective TR of about 6 s (29).

Localized first- and second-order shim terms were adjusted manually to reach a line width for the water resonance inferior to 60 Hz. For each mouse, the MRS signals were acquired without water suppression (8 accumulations, 1 min scan time) and with VAPOR (Variable Pulse Power and Optimized Relaxation delays) water suppression (128 accumulations, 7 min scan time).

Spectra without water suppression were also collected over a range of TEs from 21 to 100 ms (TE: 21/26/31/36/100 ms) in order to calculate the different spin-spin relaxation times (T₂) of the resonances of both *in vitro* and *in vivo* spectra.

For validation purposes, *in vitro* MRS measurements were also collected from one sample filled with sunflower oil, with known composition (6% methyl palmitate, 3% methyl stearate, 35% methyl oleate, 50% methyl linoleate, 3% methyl linolenate, and 3% methyl arachidate) using a unique TE PRESS sequence (TE/TR: 16/5,000 ms).

MRS data processing

The MRS signals were processed in the time domain after being corrected for zero- and first-order phase. The quantification procedure, called the Multiple Starting Value method, implemented in Matlab R2011b, is based on a nonlinear least-squares algorithm that fits the time-domain signal to a combination of Voigt model functions (30). Each Voigt function is characterized by the combination of Lorentzian and Gaussian functions. The model function used in the fitting procedure is a weighted sum of damped sinusoids which are Voigt lines after Fourier transform. The weighting factors involved in the linear combination of the different damped sinusoids are called the amplitude parameters in the time domain which is, in the frequency domain, the usual peak area. Thus, the free model parameters are the amplitudes, Lorentzian and Gaussian damping factors, and frequencies of each Voigt lineshape and the zero-order phase. The algorithm uses multiple random starting values and bounds for the frequency and damping factor parameters. The frequency parameters were constrained within an interval of ± 10 Hz around their starting values. The Lorentzian and Gaussian damping factors were constrained to be lower than 200 Hz *in vitro* and 350 Hz *in vivo*, the zero-order phase was constrained within an interval of $\pm 3^\circ$ around 0° . In this manuscript, the estimated amplitude parameter of the Voigt lineshape resonating at the frequency f is written " f " and refers also, in the interests of simplifying notation, to intensity of the resonance arising at the frequency f .

For the *in vitro* measurements, 10 resonances were identified and quantified: methyl group (0.9 ppm), methylene group (1.3 ppm), β -methylene to carboxylic group (1.6 ppm), allylic group (2 ppm), α -methylene to carboxylic group (2.25 ppm), diallylic group (2.8 ppm), glycerol backbone (4.07 ppm, 4.23 ppm, 5.2 ppm), and olefinic group (5.3 ppm).

For *in vivo* measurements, no contribution to the resonances other than lipid was assumed, since lipid resonances are predominant in MR liver spectra. Nine resonances were then identified, 5.3 ppm and 5.2 ppm being considered as a single broad resonance (Table 1). Each resonance was modeled with one component in the model-function except for 1.3 ppm, which was fitted with one or two components *in vivo* and *in vitro* and for the water at 4.7 ppm which was fitted with one or two components *in vivo*. Water amplitude was used as internal reference. Reliability of the

parameter estimates was assessed using Cramér Rao theory. Amplitude estimates with Cramér Rao lower bounds above 20% were discarded from the subsequent analysis.

Relaxation time measurements

Spectra were quantified with the same algorithm as described previously. Then, T2 decay of each resonance according to the TE was modeled with a mono-exponential decay and T2 correction was performed as described by (15). Each resonance was corrected in intensity with the corresponding estimated T2 relaxation time.

No T1 relaxation times were estimated for additional correction because for TR > 3,000 ms (*in vivo*) and TR = 5,000 ms (*in vitro*), all resonances were considered fully relaxed.

Calculation of lipid composition

The total lipid (TL) index reflects the hepatic fat content and was calculated as the relative ratio of resonance intensities from methylene and methyl chemical groups to water. Indexes of saturation and unsaturation were evaluated according to (14, 31, 32) as described in Table 2. The ratio of methylene resonance intensity to methyl resonance intensity described the saturated component (SC) of hepatic fatty acids. The fraction of unsaturation (FU) is expressed with the ratio of allylic to α -methylene to carbonylic group resonance intensities.

The amount of total unsaturation was estimated using two indexes: the total unsaturated fatty acids (TUFAs) and the total unsaturated fatty acid index (TUFU). On the one hand, TUFU was calculated as the ratio of olefinic (methine) resonance contribution to water and methylene resonance contributions. This index reflects the amount of total (poly and mono) unsaturated fatty acids relative to the water content and TL. A subsidiary index is the relative TUFU (rTUFU) which gives the TUFU relative to the amount of total fatty acids. On the other hand, TUFU was defined as the ratio of allylic to methylene resonance intensities. While TUFU is directly proportional to the number of double bonds found in the lipids presents in the volume of interest, TUFU will be directly proportional to the number of unsaturated chains, whether they are mono or poly unsaturated fatty acid chains. The ratio of olefinic resonance intensity to methyl resonance intensity is called the total unsaturated bond index (TUBI) and approximates the average number of double bonds for the unsaturated fatty acids.

GC analysis

Fatty acid assay was performed as described in (33). Following homogenization of liver samples in methanol/5 mM EGTA (2:1, v/v), lipids corresponding to an equivalent of 1 mg of liver were extracted in the presence of glyceryl triheptadecanoate (0.5 g) as an internal standard. The lipid extract was transmethylated with 1 ml of boron trifluoride in methanol (1:20, v/v) for 150 min at 100°C, evaporated to dryness, and the fatty acid methyl esters (FAMES) were extracted with hexane/water (3:1). The organic phase was evaporated to dryness and dissolved in 50 μ l ethyl acetate. One microliter of FAME was analyzed by gas-liquid chromatography on a 5890 Hewlett-Packard system using a Fawax fused-silica capillary column (30 m, 0.32 mm internal diameter, 0.25 mm film thickness; Restek, Belfast, UK). Oven temperature was programmed from 110 to 220°C at a rate of 2°C/min, and the carrier gas was hydrogen (0.5 bar). The injector and the detector were at 225 and 245°C, respectively. Identification of the FAMES was based upon retention times obtained for methyl ester standards. In order to obtain comparable results between the GC and MRS methodologies, the proportions of the chemically equivalent groups of protons were calculated from the GC fatty acid data according to (27), with normalization with each mass of

TABLE 1. Assignment of the nine chemical groups and their corresponding chemical shift from *in vivo* 1 H-MRS spectra

Chemical Group	Chemical Shift (ppm)	Description
CH ₃	0.9	Methyl
(CH ₂) _n	1.3	Methylene
CH ₂ CH ₂ CO	1.6	β -Methylene to carboxyl group
CH ₂ CH=CHCH ₂ CH ₂	2.00	Allylic
CH ₂ CH ₂ CO	2.25	α -Methylene to carboxyl group
CH=CHCH ₂ CH=CH	2.8	Diallylic (polyunsaturated)
CH ₂ -COO	4.07	Glycerol backbone
CH ₂ -COO	4.23	Glycerol backbone
CH=CH	5.3	Olefinic

Acquired in a mouse liver at 7 T (Fig. 3) with a short-TE PRESS sequence (TE/TR: 16/3,000 ms).

TABLE 2. Indexes of fatty acid composition evaluated from analysis of proton MRS spectra.

Index of Fatty Acid	Fatty Acid Component
TL	$(“1.3” + “0.9”) / (“1.3” + “0.9” + “4.7”)$
SC	$(3/2) \times (“1.3” / “0.9”)$
FU	$(1/2) \times (“2” / “2.25”)$
TUFA	$“5.3” / (“1.3” + “4.7”)$
TUFI	$(3/4) \times (“2” / “0.9”)$
TUBI	$(3/2) \times (“5.3” / “0.9”)$

The estimated amplitude of the time-domain function resonating at the frequency f is written “ f ”.

each fatty acid respectively, and then fatty acid indexes were derived.

Statistics analysis

Wilcoxon rank tests were performed to determine the statistical difference between the groups and $P = 0.05$ was considered to be significant. Correlation between MRS and GC estimated parameters were evaluated with Pearson coefficient correlation. Tukey box plots (34) were chosen for plotting data. On each box, the central mark is the median, the edges of the box are the 25th and 75th percentiles, the whiskers extend to the most extreme data points not considered outliers, and outliers are depicted with crosses. Outliers are data points that fall more than 2 SDs from the mean. All statistical analysis was performed with the statistical Toolbox of MATLAB 7.4.

RESULTS

In vitro T2 relaxation times

Table 3 shows in vitro T2 relaxation times estimated for the chemical groups of sunflower oil. T2 relaxation times vary from 18 ms at 4.07 ppm and 4.23 ppm to 49 ms at 1.3 ppm.

In vivo T2 relaxation times

In vivo T2 estimated values for each resonance and for each group of mice are reported in Table 4. Note that the number of mice (n) is different for each group of mice and each resonance because of the quantification reliability tests based on the Cramér Rao bounds (CRBs). Indeed, estimates were excluded when CRBs were found greater than the defined threshold value (20%). Several quantitative results were excluded from the study, especially from spectra acquired in mice of the standard control group.

TABLE 3. Estimated T2 relaxation times for the functional groups of sunflower oil MRS spectrum at 7 T

Chemical Shift (ppm)	Estimated T2 Relaxation Times (ms)
5.3	40.8 ± 0.1
4.23	17.5 ± 0.1
4.07	17.7 ± 0.1
2.8	48.6 ± 0.4
2.25	27.7 ± 0.6
2	34.0 ± 0.1
1.6	17.6 ± 0.3
1.3	49 ± 2
0.9	37.9 ± 0.9

Data are presented as mean \pm SE.

Statistical T2 value comparisons between groups were only performed with $n \geq 5$.

T2 relaxation times varied from 12 to 32 ms for 5.3 ppm, from 6 to 31 ms for 2.25 ppm, from 20 to 25 ms for 2 ppm, from 5 to 95 ms for 1.6 ppm, from 24 to 39 ms for 1.3 ppm, and from 24 to 29 ms to 0.9 ppm for all groups of mice. No significant difference was found for the water resonance at 4.7 ppm between all groups because estimated T2 relaxation times were around 13 ms for all mice.

T2 relaxation times of 2.25 ppm resonance were found significantly lower for *L-G6pc*^{-/-} mice fed a HF/HS diet than for control mice fed a HF/HS diet. At 1.3 ppm, T2 relaxation times were found significantly higher for *L-G6pc*^{-/-} mice fed a standard diet than control mice fed a standard diet. Significantly higher T2 values were also measured for control mice fed a HF/HS diet compared with control mice fed a standard diet.

In vitro MRS index validation

Figure 1 shows a typical MRS spectrum acquired from a sunflower oil sample. Ten resonances were identified. Theoretical and estimated values for fatty acid indexes and relative resonance intensities are reported in Table 5 and show good correlation ($R^2 = 0.97$). However, ratios in which the intensity of the resonance arising at 0.9 ppm is involved (SC, TUFI, TUBI) show the highest differences between theoretical and estimated values (relative error of estimation: $24.2 \pm 16.0\%$, mean \pm SD) compared with the ratios without any 0.9 ppm contribution (relative error of estimation: $7.1 \pm 4.3\%$).

In vivo lipid profiles estimated by MRS

Figure 2 shows typical spectra from each group of mice. On standard diet, the “1.3” ppm was higher for *L-G6pc*^{-/-} mice than for control mice. The control mice fed a HF/HS diet showed also a higher ppm than the control mice fed a standard diet. For the *L-G6pc*^{-/-} mice fed a HF/HS diet, the *L-G6pc*^{-/-} mice fed a standard diet, and the control mice fed a HF/HS diet, the resonance intensities 1.3 ppm tend to have the same level. As shown in Fig. 2 and in Fig. 3, the 2.8 ppm was very low from *L-G6pc*^{-/-} and control mice. An example of a MRS spectrum quantification using the multiple starting value method is given in Fig. 3.

The lipid profiles estimated from MRS experiments are shown in Fig. 4. On standard diet, *L-G6pc*^{-/-} mice showed higher amplitude than control mice for all resonances except 2.25 ppm. In the same way, *L-G6pc*^{-/-} mice fed a HF/HS diet showed significantly higher amplitudes than control mice fed a HF/HS diet for 2.25 and 2 ppm. No statistically significant difference was found for the other resonances. Concerning the control groups, mice fed a HF/HS diet showed statistically significant higher amplitudes than control group fed a standard diet for 5.3, 2, 1.6, 1.3, and 0.9 ppm. Besides, no statistically significant difference in any of the resonance amplitude estimates was found between a HF/HS diet and a standard diet for the *L-G6pc*^{-/-} group. Using the CRBs reliability criterion, estimated amplitudes for 2.8, 4.07, and 4.23 ppm were found mostly unreliable and were rejected from the statistical analysis.

TABLE 4. Estimated T2 relaxation time values for the four groups of mice

Group	Diet	Chemical Shift (ppm)	Estimated T2 Relaxation Time (ms)
L-G6pc ^{-/-}	HF/HS	5.3	23 ± 8 (n = 12)
	Standard	5.3	20 ± 18 (n = 15)
Control	HF/HS	5.3	32 ± 17 (n = 11)
	Standard	5.3	12 (n = 1)
L-G6pc ^{-/-}	HF/HS	4.7	13 ± 1 (n = 12)
	Standard	4.7	14 ± 2 (n = 15)
Control	HF/HS	4.7	13 ± 2 (n = 12)
	Standard	4.7	14 ± 2 (n = 5)
L-G6pc ^{-/-}	HF/HS	2.25	19 ± 10 ^{a*} (n = 12)
	Standard	2.25	19 ± 7 (n = 14)
Control	HF/HS	2.25	31 ± 11 (n = 11)
	Standard	2.25	6 (n = 1)
L-G6pc ^{-/-}	HF/HS	2	22 ± 6 (n = 12)
	Standard	2	20 ± 7 (n = 14)
Control	HF/HS	2	25 ± 6 (n = 12)
	Standard	2	21 ± 5 (n = 2)
L-G6pc ^{-/-}	HF/HS	1.6	26 ± 16 (n = 4)
	Standard	1.6	23 ± 10 (n = 4)
Control	HF/HS	1.6	95 ± 61 (n = 4)
	Standard	1.6	5 (n = 1)
L-G6pc ^{-/-}	HF/HS	1.3	39 ± 5 (n = 12)
	Standard	1.3	35 ± 8 ^{a,**} (n = 15)
Control	HF/HS	1.3	39 ± 6 ^{b,**} (n = 12)
	Standard	1.3	24 ± 3 (n = 5)
L-G6pc ^{-/-}	HF/HS	0.9	29 ± 9 (n = 12)
	Standard	0.9	26 ± 8 (n = 15)
Control	HF/HS	0.9	24 ± 8 (n = 12)
	Standard	0.9	26 ± 18 (n = 5)

Data are presented as mean ± SD. Number of mice per group (n) are in parentheses. Statistical comparisons for T2 values between groups proceeded only if n ≥ 5. **P* < 0.05, ***P* < 0.01.

^aSignificantly different from the control group.

^bSignificantly different from the standard diet.

In vivo TL estimation using MRS

The percentages of TL to the water estimated from MRS experiments for each group of mice are shown in **Fig. 5A**. On standard diet, the percentage of TL was statistically higher in L-G6pc^{-/-} mice than in control mice. No statistically significant difference was observed between L-G6pc^{-/-} mice fed a HF/HS diet and control mice fed a HF/HS diet. As expected, lipid quantity was significantly higher in control mice fed a HF/HS diet than in control mice fed a standard diet. Interestingly, no statistically significant difference between estimated lipid quantities was observed between L-G6pc^{-/-} mice fed a HF/HS diet versus a standard

diet. Moreover, these former TL quantities were in the same range as the one estimated for the control mice fed a HF/HS diet.

Hepatic TG measurements

Colorimetric measurements of TGs are provided in **Table 6**. TG was found significantly higher (*P* < 0.001) in L-G6pc^{-/-} mice fed a standard diet compared with control mice. These results are in accordance with the development of a marked steatosis in L-G6pc^{-/-} mice after 9 months of G6pc deletion. Interestingly, there was no effect of a HF/HS diet on hepatic TG content in L-G6pc^{-/-} mice.

Proton MRS spectrum of sunflower oil+fit

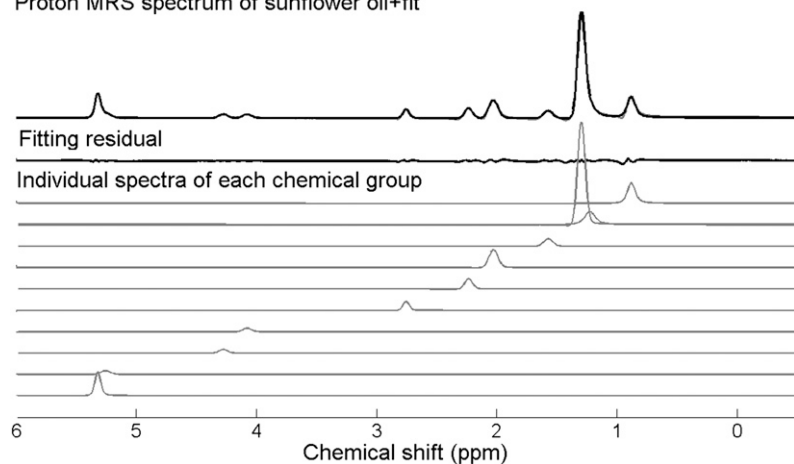


Fig. 1. ¹H-MRS spectrum of sunflower oil acquired with PRESS sequence (TE/TR: 16/5,000 ms) allowing quantification of 10 chemical groups with CRB <20%. From top to bottom: the ¹H-MRS spectrum (real spectrum and fit), the fitting residual and the individual spectra attributed to each chemical group: methyl group (0.9 ppm), methylene group (1.3 ppm), β-methylene to carboxylic group (1.6 ppm), allylic group (2 ppm), α-methylene to carboxylic group (2.25 ppm), diallylic group (2.8 ppm), glycerol backbone (5.2 ppm, 4.23 ppm, 4.07 ppm), and olefinic group (5.3 ppm). Note that the methylene resonance at 1.3 ppm was fitted with two components.

TABLE 5. Estimated index of fatty acid of sunflower oil obtained from experimentally measured ratios from MRS experiments and theoretical ratios

	1.3/1.6	2.8/2.25	2.25/1.6	1/2 × 2/1.6	SC	FU	TUFI	TUBI
Experimentally measured ratios	8.03 ± 0.29	0.55 ± 0.02	0.87 ± 0.03	0.88 ± 0.05	8.74 ± 0.11	0.88 ± 0.04	0.88 ± 0.08	1.35 ± 0.01
Theoretical ratios	8.74	0.56	1	0.81	6.38	0.92	0.63	1.44

Confidence intervals were estimated using the Cramér Rao theory.

On the contrary, TG was found significantly higher in control mice fed a HF/HS diet compared with control mice fed a standard diet. Surprisingly, TG content was found significantly lower in *L-G6pc*^{-/-} mice fed a HF/HS diet compared with control mice fed a HF/HS diet.

GC results

Fatty acid compositions of liver TLs in the four groups of mice are presented in **Table 7**. A significant decrease ($P < 0.01$) in 14:0 (myristic acid) and 16:0 (palmitic acid) was determined in the *L-G6pc*^{-/-} mice fed a HF/HS diet compared with controls fed a HF/HS diet. A significantly ($P < 0.05$) lower proportion of 16:0 and 18:0 (stearic acid) was also determined in the *L-G6pc*^{-/-} mice fed a standard diet compared with controls fed a standard diet. In contrast, the content of 16:0 in the control mice fed a HF/HS

diet was significantly higher compared with controls fed a standard diet. This change represents a significant decrease of total saturated fatty acids (SFAs) (Table 7) in *L-G6pc*^{-/-} mice compared with the corresponding controls fed the same diet (9% decrease for mice fed a standard diet and 27% decrease for mice fed a HF/HS diet). For control mice, the ones fed a HF/HS diet showed a significant increase (27%) of SFA compared with the ones fed a standard diet. In relation to the significant increase in 16:1n-9 (cis-7 hexadecanoic acid), 16:1n-7 (palmitoleic acid), and especially 18:1n-9 (oleic acid) observed in the *L-G6pc*^{-/-} mice compared with their respective controls, the total monounsaturated fatty acids (MUFAs) were significantly increased ($P < 0.01$) in the *L-G6pc*^{-/-} mice compared with their respective controls (32% increase for standard diet, 34% increase for HF/HS diet). On the

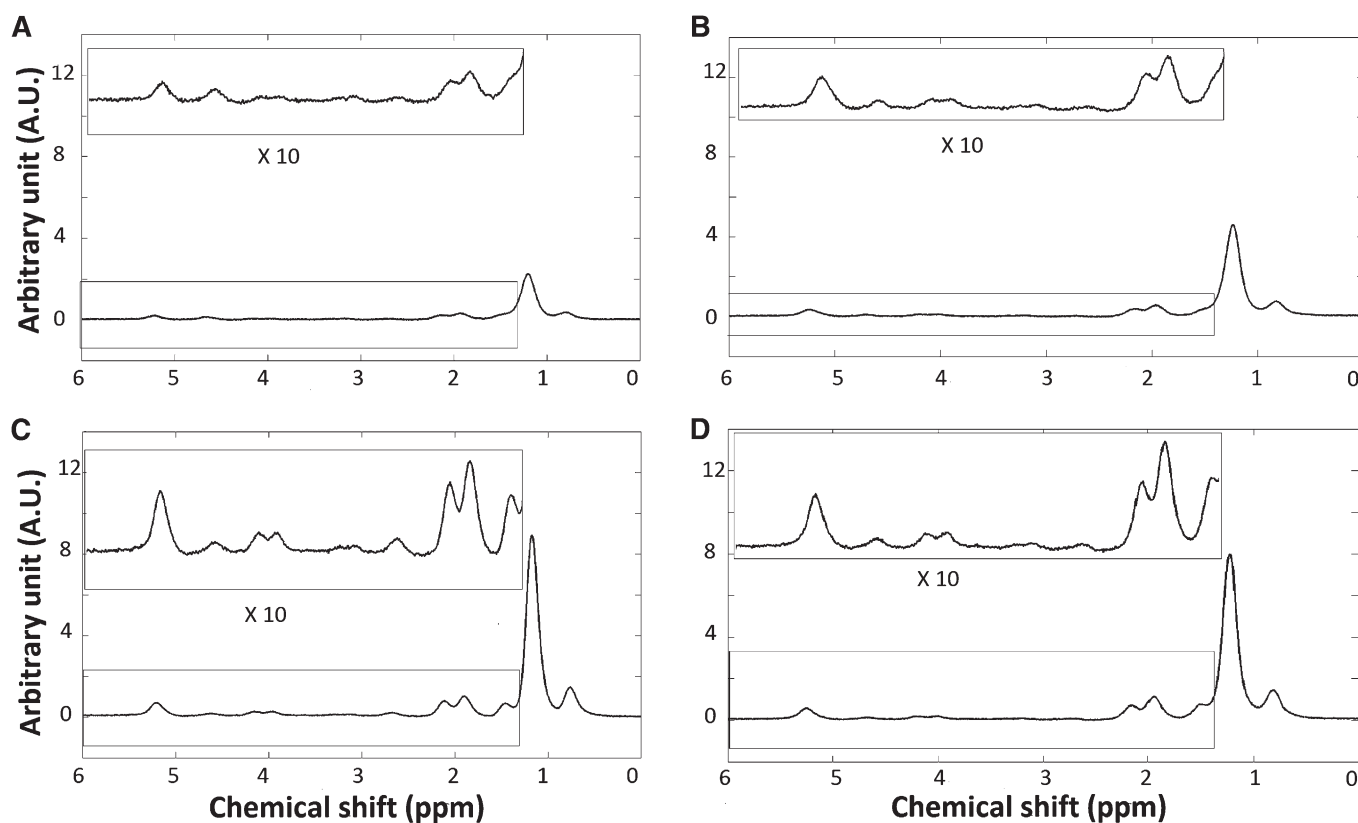


Fig. 2. Typical ¹H-MRS spectra (PRESS sequence; TE/TR: 16/3,000 ms) acquired in the liver of a mouse belonging to the: standard control group (A), standard *L-G6pc*^{-/-} group (B), HF/HS control group (C), and HF/HS *L-G6pc*^{-/-} group (D).

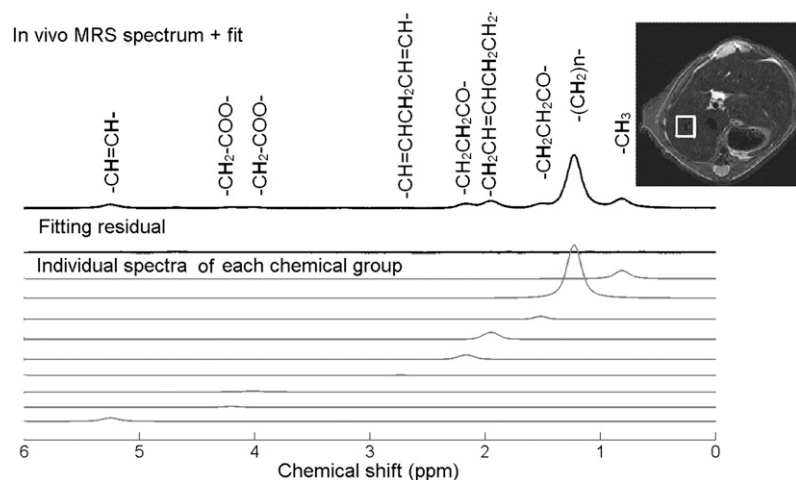


Fig. 3. In vivo proton water-suppressed spectrum acquired at 7 T within the right hepatic lobe of a control mouse fed a HF/HS diet. Nine resonances were quantified. From top to bottom: the ^1H spectrum (real spectrum and fit), the fitting residual, and the individual spectra attributed to each chemical group: methyl group (0.9 ppm), methylene group (1.3 ppm), β -methylene to carboxylic group (1.6 ppm), allylic group (2 ppm), α -methylene to carboxylic group (2.25 ppm), diallylic group (2.8 ppm), glycerol backbone (4.23 ppm), 4.07 ppm, and olefinic group (5.3 ppm). Inset: location of the voxel ($3 \times 3 \times 3 \text{ mm}^3$) in the right lobe of the mouse fed a HF/HS diet

contrary, the long-chain polyunsaturated fatty acids 20:4n-6 (arachidonic acid; 22% decrease), 20:5n-3 (eicosapentaenoic acid; 52% decrease), and 22:6n-3 (docosahexaenoic acid; 27% decrease) were significantly decreased ($P < 0.05$) in $L-G6pc^{-/-}$ mice fed a standard diet compared with control mice fed a standard diet. The latter changes represented significant, 18% ($P < 0.01$) and 29% ($P < 0.05$), decreases in total liver PUFA contents for $L-G6pc^{-/-}$ mice compared with the corresponding controls fed the same diet. Total PUFA content was also found significantly lower in control mice fed a HF/HS diet compared with control mice fed a standard diet ($P < 0.01$, 26% decrease).

In vivo SC estimation using MRS

On a standard or HF/HS diet, no significant difference of the SC was observed between $L-G6pc^{-/-}$ and control mice (Fig. 5B). Control mice fed a standard diet showed a higher level of saturated lipid compared with the estimated values for the other groups of mice.

In vivo FU estimation using MRS

FUs are shown in Fig. 5C for each group of mice. On a standard diet, the FU was significantly higher in $L-G6pc^{-/-}$ mice than in control mice ($P < 0.01$). On a HF/HS diet, no

significant difference was found between $L-G6pc^{-/-}$ and control mice. Control mice fed a HF/HS diet had a FU higher than control mice fed a standard diet. No difference was measured between $L-G6pc^{-/-}$ mice fed a HF/HS diet and $L-G6pc^{-/-}$ mice fed a standard diet.

In vivo TUFA estimation using MRS

TUFAs are shown in Fig. 5D. On a standard diet, TUFAs were higher in $L-G6pc^{-/-}$ mice than in control mice ($P = 0.06$). No significant difference was observed on a HF/HS diet. Control mice fed a HF/HS diet showed a higher TUFA than control mice fed a standard diet ($P = 0.06$). Nevertheless, no difference was found between $L-G6pc^{-/-}$ mice fed a HF/HS diet versus a standard diet.

In vivo TUF1 estimation using MRS

TUF1s are shown in Fig. 5E for each group of mice. On a standard diet, TUF1 was similar between $L-G6pc^{-/-}$ and control mice. On a HF/HS diet, TUF1 was significantly increased for $L-G6pc^{-/-}$ mice compared with control mice. In control mice, TUF1 was higher on a standard diet than on a HF/HS diet. However, no significant difference was observed between $L-G6pc^{-/-}$ mice fed a standard diet versus a HF/HS diet.

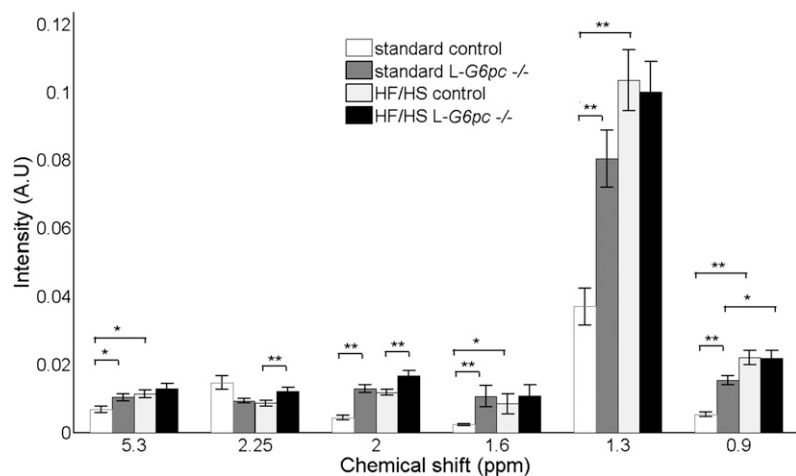


Fig. 4. MRS estimated lipid profiles for all groups (mean \pm SD): $L-G6pc^{-/-}$ mice fed a HF/HS diet (HF/HS $L-G6pc^{-/-}$, $n = 12$), $L-G6pc^{-/-}$ fed a standard diet (standard $L-G6pc^{-/-}$, $n = 15$), control mice fed a HF/HS diet (control HF/HS, $n = 12$), and control mice fed a standard diet (standard control, $n = 5$). * $P < 0.05$, ** $P < 0.01$.

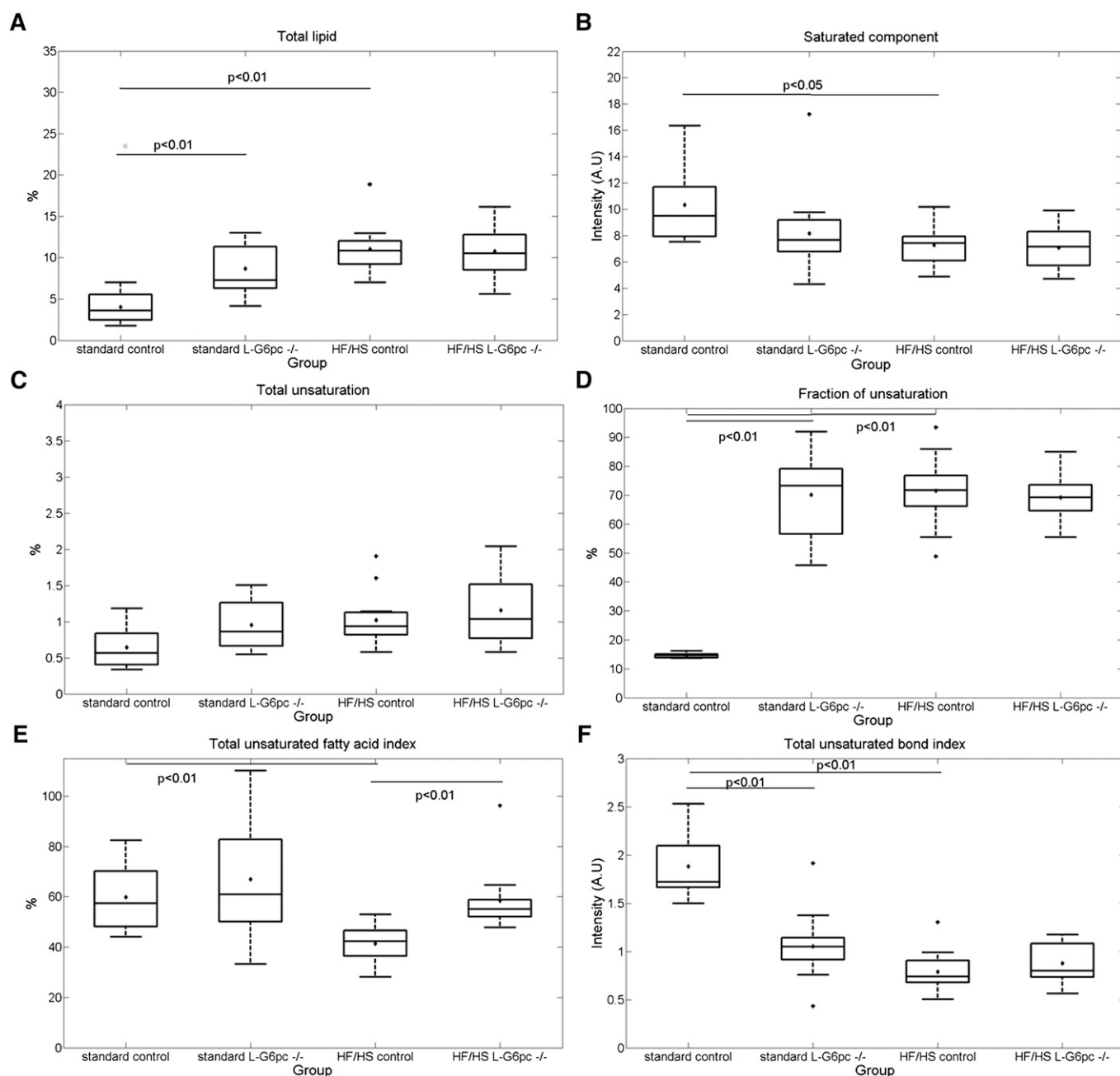


Fig. 5. Tukey box plots of the indexes derived from ¹H-MRS spectra for all groups: control mice fed a standard diet (standard control, n = 5), L-G6pc^{-/-} mice fed a standard diet (standard L-G6pc^{-/-}, n = 15), control mice fed a HF/HS diet (control HF/HS, n = 12), and L-G6pc^{-/-} mice fed a HF/HS diet (HF/HS L-G6pc^{-/-}, n = 12). Percentage of TL to water (A), SC (B), FU (C), percentage of TUFAs (D), TUFIs (E), and TUBIs (F). On each box the central mark is the median, the edges of the box are the 25th and 75th percentiles, the whiskers extend to the most extreme data points not considered outliers, and outliers are depicted as crosses. Outliers are data points that fall more than 2 SDs from the mean.

In vivo TUBI estimation using MRS

TUBIs are shown in Fig. 5F for each group of mice. On a standard diet, TUBI was significantly lower in L-G6pc^{-/-} mice than in control mice. On a HF/HS diet, no significant difference was found between L-G6pc^{-/-} and control mice. Control mice fed a HF/HS diet had a TUBI lower than control mice fed a standard diet. However, no difference was marked between L-G6pc^{-/-} mice fed a HF/HS diet and L-G6pc^{-/-} mice fed a standard diet.

Correlation between ¹H-MRS and GC lipid index estimates

A correlation coefficient of 0.52 ($P < 0.05$) was established for TUBI estimated values from MRS and GC data in mice which underwent both techniques (n = 19) without taking into consideration the groups to which they belong (Fig. 6). The MRS derived rTUFAs were correlated with GC derived rTUFAs ($r = 0.8$) without reaching statistical significance ($P > 0.05$). The MRS derived TUBI had a positive correlation with GC derived TUBI ($r = 0.45$, $P = 0.06$).

TABLE 6. Hepatic TG content in *L-G6pc*^{-/-} or control mice fed a standard diet or a HF/HS diet during 9 months

Group	Standard Diet	HF/HS Diet
Control mice	17.0 ± 1.5 (n = 5)	116.7 ± 16.8 ^{b,*} (n = 12)
<i>L-G6pc</i> ^{-/-} mice	59.7 ± 4.2 ^{a,**} (n = 15)	64.6 ± 7.2 ^{a,*} (n = 12)

Data are expressed in mg/g tissue ± SEM. The number (n) of studied mice is indicated in parentheses. **P* < 0.01, ***P* < 0.001.

^aSignificantly different from control mice.

^bSignificantly different from standard diet.

The GC and MRS measurements of the other indexes (SC and FU) did not correlate.

DISCUSSION

The aim of this study was to quantify the hepatic fat content and to determine hepatic fat composition with ¹H-MRS of mice with genetically induced steatosis (*L-G6pc*^{-/-} mice) and with diet-induced steatosis by feeding a HF/HS diet for 9 months. Such an MRS study requires some methodological choices on the MRS acquisition protocol which impact the signal to quantify. The accuracy of the quantification results primarily depends on the quality of the acquired spectra in terms of signal-to-noise ratio (SNR) and the separation of the resonating groups. The MRS quantification algorithm uses Voigt lineshape as function model. The Voigt model is appropriate for lipid quantification and yields to a better fit quality than invoking a pure Lorentzian or a pure Gaussian model (30). Moreover, the use of the Voigt model function has already proved to be suitable for quantitative in vivo spectroscopy in the brain (35, 36) and in the breast (37). As already demonstrated, the pure Lorentzian model function leads systematically to

an over-estimation of the water contribution compared with the pure Gaussian or Voigt fitting (30). Then, amplitude estimates of the time-domain functions modeling the experimentally measured MRS signals have to be corrected for transverse relaxation as the absence of correction of T2 relaxation time leads to increased lipid error estimation (38).

Working at 7 T provides a spectral dispersion that allows good ¹H lipid resonance identification and quantification. For the in vitro study, the estimated lipid profiles showed a good correlation with the theoretical values. Consequently, the proposed method was validated although the estimated relative errors for the indexes involving 0.9 ppm (SC, TUF1, and TUBI) showed moderate values. We attribute this effect to errors in the estimation of its T2 value due to signal variation with J coupling.

For in vivo experiments, respiratory gated acquisitions were set up to obtain optimal spectral resolution allowing improved quantification reliability (15). Short TE was chosen over long TE so as to minimize signal losses caused by T2 relaxation leading therefore to higher SNR. Furthermore, PRESS rather than STEAM (STimulated Echo Acquisition Mode) sequences were used so as to obtain better SNR. Nevertheless, the use of PRESS has some drawbacks. It overestimates fat and the acquired signal is more impacted by J-coupling effects (39). As a result, T2 estimation using the PRESS sequence may be influenced by the chosen TE range (40). In our case, at 7 T, the TEs were chosen to fit the expected range of T2s of all resonances. Our in vivo T2 relaxation time estimates for methyl and methylene resonances were in agreement with values reported in the literature at higher field strength (22).

In the present study, hepatic lipid content and composition were studied in mice with genetically induced steatosis

TABLE 7. Fatty acid composition of liver TMs for all groups

Fatty Acid	Standard Control (n = 8)	Standard <i>L-G6pc</i> ^{-/-} (n = 7)	HF/HS Control (n = 9)	HF/HS <i>L-G6pc</i> ^{-/-} (n = 11)
C14:0	0.33 ± 0.04	0.45 ± 0.08	1.22 ± 0.11 ^d	0.66 ± 0.04 ^b
C16:0	21.61 ± 0.45	19.50 ± 0.85 ^a	27.12 ± 0.2 ^d	16.32 ± 0.58 ^{b,c}
C16:1n-9	0.52 ± 0.03	1.23 ± 0.15 ^b	0.76 ± 0.08 ^c	1.58 ± 0.09 ^b
C16:1n-7	3.18 ± 0.16	3.02 ± 0.19	4.53 ± 0.38 ^c	1.55 ± 0.07 ^{b,d}
C18:0	9.84 ± 0.37	8.76 ± 0.73 ^a	8.56 ± 1.07	8.59 ± 0.48
C18:1n-9	27.59 ± 1.36	36.83 ± 3.76 ^b	30.93 ± 2.73	48.51 ± 1.54 ^{b,c}
C18:1n-7	4.61 ± 0.35	5.00 ± 0.29	3.51 ± 0.37	3.51 ± 0.12 ^d
C18:2n-6	13.39 ± 0.53	9.70 ± 1.59 ^b	8.20 ± 0.45 ^d	4.99 ± 0.26 ^{b,d}
C18:3n-3	0.25 ± 0.02	0.25 ± 0.04	0.29 ± 0.02	0.24 ± 0.01 ^a
C20:0	0.23 ± 0.06	0.38 ± 0.16	0.25 ± 0.11	1.38 ± 0.31 ^c
C20:1n-9	0.50 ± 0.07	0.80 ± 0.14	0.44 ± 0.07	1.00 ± 0.26
C20:2n-6	0.57 ± 0.09	0.74 ± 0.08	0.39 ± 0.04 ^c	0.61 ± 0.03 ^b
C20:3n-6	1.07 ± 0.08	1.03 ± 0.13	0.75 ± 0.08 ^c	1.01 ± 0.06 ^b
C20:4n-6	9.22 ± 0.69	7.13 ± 1.02 ^a	6.65 ± 1.02	5.26 ± 0.48
C20:5n-3	0.38 ± 0.06	0.18 ± 0.04 ^b	0.33 ± 0.05	0.11 ± 0.02 ^b
C22:6n-3	6.49 ± 0.29	4.71 ± 0.59 ^a	6.01 ± 0.83	4.06 ± 0.39
SFA	32.05 ± 2.85	29.16 ± 2.56 ^b	37.26 ± 3.48 ^d	27.00 ± 2.12 ^a
MUFA	37.79 ± 2.99	50.78 ± 3.97 ^b	43.00 ± 3.33	57.79 ± 5.36 ^{b,c}
PUFA	32.81 ± 1.35	26.60 ± 0.97 ^b	24.25 ± 0.91 ^d	17.13 ± 0.62 ^c

Data are expressed as mean ± SEM. Control mice fed a standard diet (standard control, n = 8), *L-G6pc*^{-/-} mice fed a standard diet (standard *L-G6pc*^{-/-}, n = 7), control mice fed a HF/HS diet (control HF/HS, n = 9), and *L-G6pc*^{-/-} mice fed a HF/HS diet (HF/HS *L-G6pc*^{-/-}, n = 11).

^aSignificantly different from control mice, *P* < 0.05.

^bSignificantly different from control mice, *P* < 0.01.

^cSignificantly different from standard diet, *P* < 0.05.

^dSignificantly different from standard diet, *P* < 0.01.

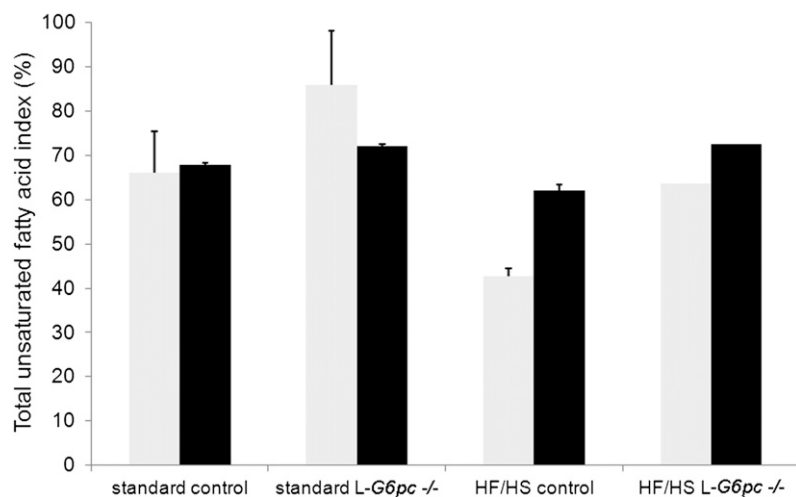


Fig. 6. TUF_I (mean ± SEM) estimated from MRS experiments (gray bars) and GC experiments (black bars) for all groups of mice without taking into consideration the groups to which they belong: control mice fed a standard diet (standard control, n = 3), L-G6pc^{-/-} mice fed a standard diet (standard L-G6pc^{-/-}, n = 6), control mice fed a HF/HS diet (control HF/HS, n = 5), and L-G6pc^{-/-} mice fed a HF/HS diet (HF/HS L-G6pc^{-/-}, n = 5).

(L-G6pc^{-/-} mice) and in mice with diet-induced steatosis by feeding a HF/HS diet for 9 months. Steatosis is described as an accumulation of TG in liver and is associated with nonalcoholic fatty liver disease (41). In clinical diagnosis, the degree of steatosis is, up to now, generally defined by histological analyses, according to the amount of hepatocytes showing fat vacuoles as mild steatosis (<30%), moderate steatosis (<60%), and severe steatosis (>60%). ¹H-MRS allows the estimation of the percentage of TL and discrimination between the stages of steatosis. A TL content greater than 5% defines steatosis according to (42) and the different grades of steatosis are well correlated with TLs ($r = 0.93$, $P < 0.0001$) (43). In this study, the percentage of lipid content measured by MRS was found to be higher than 5% but below 30% for the control mice fed a HF/HS diet (10.11% mean value) as well as for the two groups of L-G6pc^{-/-} mice fed the standard diet (8.42% mean value) and the HF/HS diet (10.34% mean value). Thus the studied steatosis is graded as mild steatosis, making a specificity of this study. The liver TG levels obtained using biochemical assay, although similarly revealing marked steatosis for the three mentioned groups of mice, do not correlate with lipid content obtained by MRS. Indeed, we observed very different variabilities of the TG measurements with the colorimetric assay compared with MRS measurements. While the L-G6pc^{-/-} mice fed a standard diet showed SEM at 7% of the mean value for the TG measurement, SEM was at 24% of the mean value for the MRS measurement. Reversely, in the control mice fed a HF/HS diet, SEM was at 10% of the mean value for the MRS measurement and was at 22% of the mean value for the TG measurement. This variability is attributed to sampling error (part of the liver retained for the TG measurements and voxel position for the MRS measurement) due to inhomogeneity in the distribution of TG in the liver. As expected, control mice fed a HF/HS diet developed liver steatosis. L-G6pc^{-/-} mice also developed steatosis but independently of the diet. The lipid content estimated in L-G6pc^{-/-} mice fed a standard diet was already high and similar to that measured in control mice fed a HF/HS diet. These results were expected as previous histological findings revealed that the L-G6pc^{-/-} mouse model showed

marked steatosis with no fibrosis marker (5). An in-depth description of the metabolic effects encountered in this model is provided by Mutel et al. (5). The hepatic steatosis encountered in L-G6pc^{-/-} mice is periportal whereas it is known that steatosis associated with obesity is rather localized around the central vein. In this model, the major modifications concern the hepatic lipid and carbohydrate metabolism because of the strong accumulation of glucose-6-phosphate in the liver. This induces the activation of the ChREBP factor and activation of the glycolysis, glycogen synthesis, and de novo lipogenesis that resulted in hepatomegaly and steatosis for this mouse model fed a standard diet (5). Unexpectedly, our results suggested that a HF/HS diet did not aggravate steatosis of L-G6pc^{-/-} mice because they did not accumulate more hepatic lipids. This observation has to be linked to the specific lipid composition obtained from GC of the liver of these mice, increase of the oleic acid (protective effect) and decrease of the palmitate (cellular toxicity). A similar lipid profile has been observed in mice overexpressing ChREBP that increased accumulation of MUFAs (11).

From the T₂ relaxation times estimation, it was observed that, the spin-spin relaxation times of the different functional groups of the lipid chains tend to increase with steatosis and were found higher for groups of mice developing steatosis (L-G6pc^{-/-} mice fed the two diets and control) than in control mice, with a significant difference for the methylene resonance (1.3 ppm). In contrast, no significant difference in T₂ was found for the water resonance. Correction for T₂ effects of the water and methylene contributions is highly required not to overestimate the lipid content (38, 44). To our knowledge, very few works have studied or reported whether T₂ values vary with steatosis level (45, 46), as most of the studies assume a constant T₂ value for lipid and water. In (22), a significant increase of the T₂ value was found for the methyl group rather than for the methylene group. For the other lipid resonance, whether or not the peak area estimates should be corrected for T₂ is more debatable. In this study we chose to correct all the compounds for T₂, with mean values estimated for each group. Indeed the systematic accurate estimation of T₂ for each resonance, at each TE, and for each

mouse was not always possible. We used the Cramér Rao theory to evaluate the reliability of each estimation with a more restrictive threshold (20%) than suggested by Kreis (47) (50%), several amplitude estimates were rejected and not used for the subsequent estimation of T2 relaxation times (requiring at least 5 reliable data points for fitting). As the result, most of the rejected estimates were evaluated from spectra of control mice fed a standard diet leading to very few reliable T2 relaxation time estimates for this group. The T2 estimations were particularly difficult for the control mice as their spectra showed very low SNRs due to their low fat content. Also, for this group, some estimated T2 values were inordinately short. For these control mice, we maintained the assumption that there is no contribution to the spectrum resonances from components other than lipids, as no particular modifications were required in the model function used to fit these data. Nonetheless, some metabolite contributions might be non-negligible and this specific problem would require further investigations.

From very recent studies, ^1H -MRS has proved to be able to provide interesting insight into the lipid composition. Several indexes, calculated as ratio of the contribution of the individual spectral component, have been proposed in the literature, and this work proposes to determine most of them to study their performance and the difficulties to assess them. Nonetheless, the direct analysis of the lipid profiles already provides substantial information. Higher estimated contribution for olefinic protons (5.3 ppm) in $L-G6pc^{-/-}$ mice fed a standard diet than in control mice fed a standard diet was found. Similar observations were also found in a hepatocarcinogenesis in a rat model (48), as well in an animal model of gliomas (49). As this mouse model develops adenomas as reported in (5), this increase is coherent. It is also consistent with GC measurements. These results reconfirm that the $L-G6pc^{-/-}$ mouse model is a well-suited model for studying both steatosis and tumor developments. The allylic protons (2 ppm), also linked to unsaturation of fatty acids, showed a significant increase in $L-G6pc^{-/-}$ mice compared with their respective controls. The methylene protons (1.3 ppm), for their part, and as already well-known, appropriately reflect the TG levels. In this study, the resonance intensity of diallylic protons (2.8 ppm) was shown to be at a very low level (Fig. 2), making their quantification almost systematically unreliable in accordance with the CRBs threshold. The diallylic protons are directly linked to the polyunsaturation of fatty acids, which has been reported to be related to lobular inflammation (31). From GC measurements, the PUFAs significantly decreased in the mouse model compared with the control, and in the control mice fed a HF/HS diet compared with the control mice fed a standard diet. Thus, consistently with GC results, the 2.8 ppm resonance was fairly undetectable in the studied fatty livers.

When analyzing MRS quantitative profiles, it is advisable, as much as possible, to make thorough checks and take precautions not to misinterpret changes. In this work, the water contribution was used as internal reference. Some studies have suggested that water content may depend

on steatosis degree, as it decreased with mild and moderate steatosis (43). In the present study, the T2 values of the water resonance between the different groups of mice did not differ significantly. As a result, it is a reasonable assumption that no alteration of the liver tissue due, for example, to fibrosis has occurred, and that the water content has not been affected in the observed grade of steatosis. Moreover, in our experiments the VAPOR module for water suppression was used to get a more accurate fitting of the lipid components than when using water-unsuppressed spectra. This was particularly true when studying control mice fed a standard diet.

Most of the MRS indexes characterizing the unsaturation of the liver fatty acids (TUFI, TUFA, and TUBI) in the mouse model, and for the two diets, were consistent with GC. Indeed, the average number of double bonds per chain given by TUBI was found significantly lower in $L-G6pc^{-/-}$ mice fed a standard diet compared with control mice fed a standard diet. This is in accordance with GC as both decrease of PUFAs and increase of MUFAs contribute to reduce this index to around one (1.05 mean value). Note that an increase of the SFAs also would result in a TUBI reduction. The two groups fed a HF/HS diet showed a TUBI below one. This could be interpreted as a greater amount of SFA compared with the group of mice fed a standard diet although GC reports an increase of SFA only for the control mice fed a HF/HS diet and rather a decrease for the mouse model. In other studies, the TUBI was reported to be higher in animal models of fibrosis (25) or steatohepatitis (14) than baseline controls. Here $L-G6pc^{-/-}$ mice did not show any fibrosis marker (5). In this study, TUBI was significantly lower in the mice developing steatosis compared with control mice fed a standard diet. The SC also is indirectly an indicator of the proportion of unsaturated chains relative to saturated chains. Indeed the ratios of the methylene group contribution over the methyl group contribution range from 10 to 16 for a saturated chain, from 8 to 12 for a monounsaturated chain, and from 0 to 9 for a polyunsaturated chain. A significant decrease of SC was found here for control mice fed a HF/HS diet compared with control mice fed a standard diet. SC and TUBI are two indexes that have to be examined together in order to assess the modification in content of SFAs. In our case, we hypothesize that these indexes are slightly underestimated for the three groups developing steatosis due to an underestimation of the T2 value of the methyl resonance leading to an overestimation of its contribution. The decrease in SC is seen as resulting from an increase of the MUFAs compared with SFAs.

TUFA, directly related to the number of double bonds and reflecting the TUFAs relative to the water and lipid content, was found higher in $L-G6pc^{-/-}$ mice fed a standard diet compared with control mice fed a standard diet, and also in control mice fed a HF/HS diet compared with control mice fed a standard diet, but without being significant ($P=0.06$). This index was also estimated in a study of steatosis induced by choline- or methionine-choline-deficient diets in a rat model (31), and was found

to significantly increase according to the diet follow-up. In the present study, the proportion of TUFAs relative to the amount of total fatty acids [rTUFA, “5.4”/“1.3” ppm (31)] measured with ^1H -MRS was correlated with GC-derived index ($r = 0.8$) without reaching statistical significance ($P > 0.05$). TUFU, directly related to the number of unsaturated fatty acid chains, was significantly higher in $L-G6pc^{-/-}$ mice fed a HF/HS diet compared with control mice fed a HF/HS diet, consistent with GC in which the TUFAs (sum of PUFAs and MUFAs) increased significantly in the mouse model groups compared with their respective control groups. A moderate but statistically significant correlation ($r = 0.52$) for TUFU has been estimated between GC and MRS measurements. In (14), a hepatic necroinflammatory response was described as inducing an increase in TUFU which might explain the increase of this index in this study. No histopathological examinations were performed to confirm this hypothesis. FU calculated as the ratio of allylic to α -methylene to carboxylic group did not show any difference between the groups of mice. When correcting contributions with measured T2 values, the control mice presented an unrealistic estimated FU, encouraging to consider for this index the estimate obtained from the contributions without T2 correction.

As opposed to GC, the interpretation of MRS indexes is not always straightforward. Indeed for some resonance contributions and/or indexes, the observed changes are due to the cumulative effect of changes in saturated, monounsaturated, and polyunsaturated fatty acids. This is the case for indexes involving the olefinic resonance at 5.3 ppm (TUBI, TUFA, rTUFA) and the methylene resonance at 1.3 ppm (SC index). The MRS technique is sensitive only to molecules with a high degree of rotational molecular motion. The lipid resonances arise only from TGs in intracellular fat droplets and lipids in membrane bilayer conformation (mainly phospholipids) are not detectable using NMR techniques (14). It should be noticed that, the GC analysis was performed without any selective analysis of major classes of lipids (TG, phospholipid, cholesterol). As the result, in this study dealing with mild steatosis, the two technique measurements were not highly correlated while the trends were in agreement.

CONCLUSION

In vivo ^1H -MRS is a powerful technique to noninvasively assess lipid composition and lipid content in mouse liver. The estimation of hepatic lipid indexes related to fatty acid unsaturation fractions was performed to follow genetically induced and diet-induced steatosis. The percentage of TL to water measured by MRS enabled the encountered steatosis to be graded as mild steatosis, and the TUFU, directly related to the number of unsaturated fatty acids chains, enabled to discriminate between the genetically induced steatosis and diet-induced steatosis. 

The authors thank Kevin Tse Ve Koon for help in editing the manuscript and the staff members of the Genotoul (Toulouse) Lipidomic core facility (Metatoul-Lipidomique) for technical

assistance with GC analysis. The MRS experiments were performed by the authors using the MRI system available on CERMEP imagerie du vivant, Bron, F-69677, France, imaging facilities.

REFERENCES

1. Chou, J. Y., H. S. Jun, and B. C. Mansfield. 2010. Glycogen storage disease type I and G6Pase- β deficiency: etiology and therapy. *Nat. Rev. Endocrinol.* **6**: 676–688.
2. Froissart, R., M. Piraud, A. M. Boudjemline, C. Vianey-Saban, F. Petit, A. Hubert-Buron, P. T. Eberschweiler, V. Gajdos, and P. Labrune. 2011. Glucose-6-phosphatase deficiency. *Orphanet J. Rare Dis.* **6**: 27.
3. Rake, J. P., G. Visser, P. Labrune, J. V. Leonard, K. Ullrich, and G. P. Smit. 2002. Glycogen storage disease type I: diagnosis, management, clinical course and outcome. Results of the European Study on Glycogen Storage Disease Type I (ESGSD I). *Eur. J. Pediatr.* **161**: S20–S34.
4. Heller, S., L. Worona, and A. Consuelo. 2008. Nutritional therapy for glycogen storage diseases. *J. Pediatr. Gastroenterol. Nutr.* **47**: S15–S21.
5. Mutel, E., A. Abdul-Wahed, N. Ramamonjisoa, A. Stefanutti, I. Houberton, S. Cavassila, F. Pilleul, O. Beuf, A. Gautier-Stein, A. Penhoat, et al. 2011. Targeted deletion of liver glucose-6-phosphatase mimics glycogen storage disease type Ia including development of multiple adenomas. *J. Hepatol.* **54**: 529–537.
6. Donnelly, K. L., C. I. Smith, S. J. Schwarzenberg, J. Jessurun, M. D. Boldt, and E. J. Parks. 2005. Sources of fatty acids stored in liver and secreted via lipoproteins in patients with nonalcoholic fatty liver disease. *J. Clin. Invest.* **115**: 1343–1351.
7. Postic, C., and J. Girard. 2008. The role of the lipogenic pathway in the development of hepatic steatosis. *Diabetes Metab.* **34**: 643–648.
8. Matsuzaka, T., A. Atsumi, R. Matsumori, T. Nie, H. Shinozaki, N. Suzuki-Kemuriyama, M. Kuba, Y. Nakagawa, K. Ishii, M. Shimada, et al. 2012. Elov6 promotes nonalcoholic steatohepatitis. *Hepatology.* **56**: 2199–2208.
9. Ricchi, M., M. R. Odoardi, L. Carulli, C. Anzivino, S. Ballestri, A. Pinetti, L. I. Fantoni, F. Marra, M. Bertolotti, S. Banni, et al. 2009. Differential effect of oleic and palmitic acid on lipid accumulation and apoptosis in cultured hepatocytes. *J. Gastroenterol. Hepatol.* **24**: 830–840.
10. Tardif, N., J. Salles, J. F. Landrier, I. Mothe-Satney, C. Guillet, C. Boue-Vaysse, L. Combaret, C. Giraudet, V. Patrac, J. Bertrand-Michel, et al. 2011. Oleate-enriched diet improves insulin sensitivity and restores muscle protein synthesis in old rats. *Clin. Nutr.* **30**: 799–806.
11. Benhamed, F., P. D. Denechaud, M. Lemoine, C. Robichon, M. Moldes, J. Bertrand-Michel, V. Ratzu, L. Serfaty, C. Housset, J. Capeau, et al. 2012. The lipogenic transcription factor ChREBP dissociates hepatic steatosis from insulin resistance in mice and humans. *J. Clin. Invest.* **122**: 2176–2194.
12. Kotronen, A., T. Seppänen-Laakso, J. Westerbacka, T. Kiviluoto, J. Arola, A. L. Ruskeepää, H. Yki-Järvinen, and M. Oresic. 2010. Comparison of lipid and fatty acid composition of the liver, subcutaneous and intra-abdominal adipose tissue, and serum. *Obesity (Silver Spring).* **18**: 937–944.
13. Ratzu, V., F. Charlotte, A. Heurtier, S. Gombert, P. Giral, E. Bruckert, A. Grimaldi, F. Capron, and T. Poynard. 2005. Sampling variability of liver biopsy in nonalcoholic fatty liver disease. *Gastroenterology.* **128**: 1898–1906.
14. Corbin, I. R., E. E. Furth, S. Pickup, E. S. Siegelman, and E. J. Delikatny. 2009. In vivo assessment of hepatic triglycerides in murine non-alcoholic fatty liver disease using magnetic resonance spectroscopy. *Biochim. Biophys. Acta.* **1791**: 757–763.
15. Garbow, J. R., X. Lin, N. Sakata, Z. Chen, D. Koh, and G. Schonfeld. 2004. In vivo MRS measurement of liver lipid levels in mice. *J. Lipid Res.* **45**: 1364–1371.
16. Mosconi, E., M. Fontanella, D. M. Sima, S. Van Huffel, S. Fiorini, A. Sbarbati, and P. Marzola. 2011. Investigation of adipose tissues in Zucker rats using in vivo and ex vivo magnetic resonance spectroscopy. *J. Lipid Res.* **52**: 330–336.
17. Branca, R. T., and W. S. Warren. 2011. In vivo NMR detection of diet-induced changes in adipose tissue composition. *J. Lipid Res.* **52**: 833–839.

18. Ye, Q., C. F. Danzer, A. Fuchs, W. Krek, T. Mueggler, C. Baltes, and M. Rudin. 2011. Longitudinal evaluation of intramyocellular lipids (IMCLs) in tibialis anterior muscle of ob/ob and ob/+ control mice using a cryogenic surface coil at 9.4 T. *NMR Biomed.* **24**: 1295–1301.
19. Calderan, L., P. Marzola, E. Nicolato, P. F. Fabene, C. Milanese, P. Bernardi, A. Giordano, S. Cinti, and A. Sbarbati. 2006. In vivo phenotyping of the ob/ob mouse by magnetic resonance imaging and ¹H-magnetic resonance spectroscopy. *Obesity (Silver Spring)*. **14**: 405–414.
20. Lee, H. S., Q. Y. Cai, K. N. Min, J. K. Park, T. H. Kwak, K. H. Jeong, and K. S. Hong. 2010. In vivo monitoring of treatment effect of cryptotanshinone for non-alcoholic fatty liver disease in mice (Abstract in ISMRM-ESMRMB Joint Annual Meeting, Stockholm, Sweden, May 1–7, 2010).
21. Peng, X. G., S. Ju, Y. Qin, F. Fang, X. Cui, G. Liu, Y. Ni, and G. J. Teng. 2011. Quantification of liver fat in mice: comparing dual-echo Dixon imaging, chemical shift imaging, and ¹H-MR spectroscopy. *J. Lipid Res.* **52**: 1847–1855.
22. Ye, Q., C. F. Danzer, A. Fuchs, C. Wolfrum, and M. Rudin. 2012. Hepatic lipid composition differs between ob/ob and ob/+ control mice as determined by using in vivo localized proton magnetic resonance spectroscopy. *MAGMA*. **25**: 381–389.
23. Ackerman, Z., M. Oron-Herman, M. Grozovski, T. Rosenthal, O. Pappo, G. Link, and B. A. Sela. 2005. Fructose-induced fatty liver disease: hepatic effects of blood pressure and plasma triglyceride reduction. *Hypertension*. **45**: 1012–1018.
24. Gauthier, M. S., R. Favier, and J. M. Lavoie. 2006. Time course of the development of non-alcoholic hepatic steatosis in response to high-fat diet-induced obesity in rats. *Br. J. Nutr.* **95**: 273–281.
25. Cheung, J. S., S. J. Fan, D. S. Gao, A. M. Chow, J. Yang, K. Man, and E. X. Wu. 2011. In vivo lipid profiling using proton magnetic resonance spectroscopy in an experimental liver fibrosis model. *Acad. Radiol.* **18**: 377–383.
26. Kuhlmann, J., C. Neumann-Haefelin, U. Belz, J. Kalisch, H. P. Juretschke, M. Stein, E. Kleinschmidt, W. Kramer, and A. W. Herling. 2003. Intramyocellular lipid and insulin resistance: a longitudinal in vivo ¹H-spectroscopic study in Zucker diabetic fatty rats. *Diabetes*. **52**: 138–144.
27. Lundbom, J., A. Hakkarainen, B. Fielding, S. Soderlund, J. Westerbacka, M. R. Taskinen, and N. Lundbom. 2010. Characterizing human adipose tissue lipids by long echo time (1)H-MRS in vivo at 1.5 Tesla: validation by gas chromatography. *NMR Biomed.* **23**: 466–472.
28. Moraes, R. C., A. Blondet, K. Birkenkamp-Demtroeder, J. Tirard, T. F. Orntoft, A. Gertler, P. Durand, D. Naville, and M. Begeot. 2003. Study of the alteration of gene expression in adipose tissue of diet-induced obese mice by microarray and reverse transcription-polymerase chain reaction analyses. *Endocrinology*. **144**: 4773–4782.
29. Baboi, L., F. Pilleul, L. Milot, C. Lartizien, G. Poncet, C. Roche, J. Y. Scoazec, and O. Beuf. 2010. Magnetic resonance imaging follow-up of liver growth of neuroendocrine tumors in an experimental mouse model. *Magn. Reson. Imaging*. **28**: 264–272.
30. Ratiney, H., A. Bucur, M. Sdika, O. Beuf, F. Pilleul, and S. Cavassila. 2008. Effective Voigt model estimation using multiple random starting values and parameter bounds settings for in vivo hepatic ¹H magnetic resonance spectroscopic data (Abstract in 2008 IEEE International Symposium on Biomedical Imaging: From Nano to Macro, Paris, France, May 14–17, 2008).
31. van Werven, J. R., H. A. Marsman, A. J. Nederveen, F. J. Ten Kate, T. M. van Gulik, and J. Stoker. 2012. Hepatic lipid composition analysis using 3.0-T MR spectroscopy in a steatotic rat model. *Magn. Reson. Imaging*. **30**: 112–121.
32. Cobbold, J. F., J. H. Patel, R. D. Goldin, B. V. North, M. M. Crossey, J. Fitzpatrick, M. Wylezinska, H. C. Thomas, I. J. Cox, and S. D. Taylor-Robinson. 2010. Hepatic lipid profiling in chronic hepatitis C: an in vitro and in vivo proton magnetic resonance spectroscopy study. *J. Hepatol.* **52**: 16–24.
33. Zadavec, D., A. Brolinson, R. M. Fisher, C. Carneheim, R. I. Csikasz, J. Bertrand-Michel, J. Boren, H. Guillou, M. Rudling, and A. Jacobsson. 2010. Ablation of the very-long-chain fatty acid elongase ELOVL3 in mice leads to constrained lipid storage and resistance to diet-induced obesity. *FASEB J.* **24**: 4366–4377.
34. Tukey, J. W. 1977. *Exploratory Data Analysis*. Addison-Wesley, Reading, MA.
35. Marshall, I., J. Higinbotham, S. Bruce, and A. Freise. 1997. Use of Voigt lineshape for quantification of in vivo ¹H spectra. *Magn. Reson. Med.* **37**: 651–657.
36. Gillies, P., I. Marshall, M. Asplund, P. Winkler, and J. Higinbotham. 2006. Quantification of MRS data in the frequency domain using a wavelet filter, an approximated Voigt lineshape model and prior knowledge. *NMR Biomed.* **19**: 617–626.
37. Bolan, P. J., S. Meisamy, E. H. Baker, J. Lin, T. Emory, M. Nelson, L. I. Everson, D. Yee, and M. Garwood. 2003. In vivo quantification of choline compounds in the breast with ¹H MR spectroscopy. *Magn. Reson. Med.* **50**: 1134–1143.
38. Sharma, P., D. R. Martin, N. Pineda, Q. Xu, M. Vos, F. Anania, and X. Hu. 2009. Quantitative analysis of T2-correction in single-voxel magnetic resonance spectroscopy of hepatic lipid fraction. *J. Magn. Reson. Imaging*. **29**: 629–635.
39. Hamilton, G., M. S. Middleton, M. Bydder, T. Yokoo, J. B. Schimmer, Y. Kono, H. M. Patton, J. E. Lavine, and C. B. Sirlin. 2009. Effect of PRESS and STEAM sequences on magnetic resonance spectroscopic liver fat quantification. *J. Magn. Reson. Imaging*. **30**: 145–152.
40. Yahya, A., and B. G. Fallone. 2010. T(2) determination of the J-coupled methyl protons of lipids: in vivo illustration with tibial bone marrow at 3 T. *J. Magn. Reson. Imaging*. **31**: 1514–1521.
41. Contos, M. J., and A. J. Sanyal. 2002. The clinicopathologic spectrum and management of nonalcoholic fatty liver disease. *Adv. Anat. Pathol.* **9**: 37–51.
42. Szczepaniak, L. S., P. Nurenberg, D. Leonard, J. D. Browning, J. S. Reingold, S. Grundy, H. H. Hobbs, and R. L. Dobbins. 2005. Magnetic resonance spectroscopy to measure hepatic triglyceride content: prevalence of hepatic steatosis in the general population. *Am. J. Physiol. Endocrinol. Metab.* **288**: E462–E468.
43. Marsman, H. A., J. R. van Werven, A. J. Nederveen, F. J. Ten Kate, M. Heger, J. Stoker, and T. M. van Gulik. 2010. Noninvasive quantification of hepatic steatosis in rats using 3.0 T ¹H-magnetic resonance spectroscopy. *J. Magn. Reson. Imaging*. **32**: 148–154.
44. Ren, J., I. Dimitrov, A. D. Sherry, and C. R. Malloy. 2008. Composition of adipose tissue and marrow fat in humans by ¹H NMR at 7 Tesla. *J. Lipid Res.* **49**: 2055–2062.
45. Pineda, N., P. Sharma, Q. Xu, X. Hu, M. Vos, and D. R. Martin. 2009. Measurement of hepatic lipid: high-speed T2-corrected multi-echo acquisition at ¹H MR spectroscopy—a rapid and accurate technique. *Radiology*. **252**: 568–576.
46. Gilman, A. J., A. Qayyum, M. Nystrom, and S. M. Noworolski. 2011. Liver fat and water MR T2 values at 3T: dependence upon steatosis level (Abstract in 19th Annual ISMRM Scientific Meeting and Exhibition, Montreal, Canada, May 7–13, 2011).
47. Kreis, R. 2004. Issues of spectral quality in clinical ¹H-magnetic resonance spectroscopy and a gallery of artifacts. *NMR Biomed.* **17**: 361–381.
48. Foley, L. M., R. A. Towner, and D. M. Painter. 2001. In vivo image-guided (1)H-magnetic resonance spectroscopy of the serial development of hepatocarcinogenesis in an experimental animal model. *Biochim. Biophys. Acta*. **1526**: 230–236.
49. Griffin, J. L., K. K. Lehtimäki, P. K. Valonen, O. H. Grohn, M. I. Kettunen, S. Ylä-Herttuala, A. Pitkanen, J. K. Nicholson, and R. A. Kauppinen. 2003. Assignment of ¹H nuclear magnetic resonance visible polyunsaturated fatty acids in BT4C gliomas undergoing ganciclovir-thymidine kinase gene therapy-induced programmed cell death. *Cancer Res.* **63**: 3195–3201.